Lockheed
MISSILES
& SPACE
COMPANY,
INC.

HUNTSVILLE RESEARCH & ENGINEERING CENTER • P O BOX 1103 • HUNTSVILLE ALABAMA • 35807

In reply refer to:
LMSC-HREC PR D390426
7 November 1974

National Aeronautics and Space Administration
George C. Marshall Space Flight Center
Marshall Space Flight Center, Alabama 35812

Attention: AP13-F; Ray Weems, Contract Manager

Subject: Contract NAS8-26642, "Study of Multilayered Insulation Pipe Penetration," and "Thermal Acoustic Oscillation," Quarterly Progress Report

Report Period: 26 July through 25 October 1974

Gentlemen:

This letter is submitted in accordance with the provisions of Exhibit C of the subject contract and describes the direction of effort and accomplishments for the period shown above. This study is being performed by personnel in the Thermodynamics & Structures Section of the Lockheed-Huntsville Research & Engineering Center. The Contracting Officer's Representative (COR) for this contract is Mr. E. Haschal Hyde, EP43.

Discussion

- Study of Multilayered Insulation Pipe Penetration

The agreement between the analytical predictions of the net heat leak to a stored cryogen (LN_2) caused by a metal penetration through the blanket of multilayer insulation and the experimental results as modeled was shown in progress report LMSC-HREC PR D390395 to be excellent. For brevity, a single example is shown again in this report for discussion purposes. The example shown (Fig. 1) is for a 7.62 cm o.d. stainless steel pipe with a wall thickness of 0.216 cm. The penetration was insulated over a 91.4 cm length with a 2.54 cm thickness blanket. The cryogen storage vessel is aluminum with the exception of a stainless steel access port on the opposite side from the penetration. All penetrations tested were stainless steel except for two fiberglass overwrapped Inconel units. The penetrations are mounted on individual stainless steel flanges which are bolted to the cryogen tank.

Figure 1 shows that the mating surface temperature equilibrated at approximately 86°K instead of the LN_2 temperature of 77.4°K (the cryogen tank is

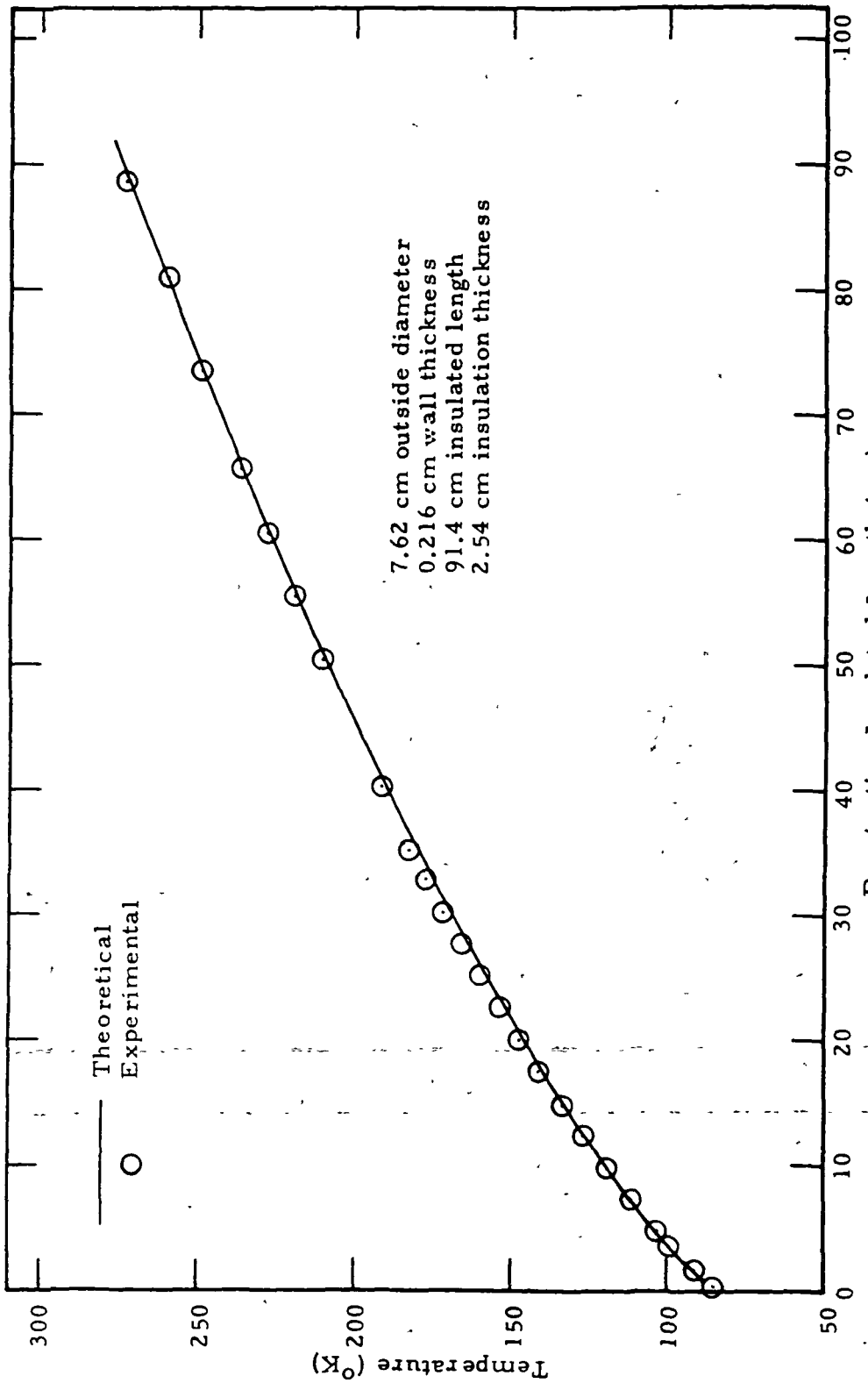

Fig. 1 - Comparison of Theoretical and Experimental Temperature Distribution on 7.62 x 0.216 x 91.4 cm Penetration

maintained at a constant 1 01 atmosphere) The differential in the equilibrium temperature is caused by a contact resistance between the flange/cryostat mounting surface. Extensive efforts were made to minimize this contact resistance, with the results being in the range of 5 to 9°K. This parameter has a direct effect on the total efficiency of the system and the resultant boil-off rate of the cryogen.

Other parameters which must be considered in the analysis of the penetration systems are the end temperature of the penetration, the diameter and wall thickness of the penetrations, the material used for the penetration, the insulation length and thickness and the cryogen being stored.

The results shown in Fig. 1 indicate very well the capability of the analytical model as now programmed to predict the system being used as the experimental verification of the model. Due to the limited flexibility as planned for the computer program for checkout purposes, variables including cryogen and penetration material properties were not originally coded into the program. That effort is now being undertaken with initiation of the final results for all these variables anticipated to begin during the November-December performance period. The computer program will then be executed for the following variables.

- Cryogen
- Penetration material
- Penetration insulated length
- Penetration insulation thickness
- Contact resistance
- Penetration temperature at end of penetration insulation
- Penetration diameter
- Penetration wall thickness
- Penetration radiation properties

The cryogens to be investigated include helium, hydrogen and oxygen. The cryogen storage container will at all times be assumed to be aluminum. The penetration materials analyzed will include stainless steel, fiberglass and Inconel. Insulation lengths and thickness will be varied over typical application ranges, as will the diameter and wall thicknesses of the penetrations analyzed. The contact resistance will be varied between the limits of 0°K drop (limiting case) to 20°K. The temperature of the penetration surface at the end of the insulation blanket will be varied depending on the insulation length and cryogen, with a judgment value being used which will be based on the results of the analytical/experimental verification program and the cryogen. This is necessary because of the large range in stored cryogen temperatures being considered (helium = 4°K, hydrogen = 20°K and oxygen = 90°K).

The surface finishes of the penetrations will be assumed to be polished with the exception of the fiberglass. Typical radiation properties of these materials for polished (metal) or "as produced" (fiberglass) will be used. Temperature-dependent conductivity values will also be incorporated.

The computer program is presently being modified to include the necessary properties of the various materials in either equation or table look-up form, depending on that property required.

Results of these analytical investigations, which will ultimately lead to a handbook form of penetration results, will be reported on as they become available.

- Thermal Acoustic Oscillations Analytical Study

The purpose of this study is to develop analytical models for predicting the effect and magnitudes of thermoacoustic oscillations on the penetration heat leak to cryogens and to experimentally verify these models. The oscillations develop as a result of large thermal gradients imposed on a compressible fluid. The expansions and compressions of the fluid generate pressure waves in much the same manner as pushing a piston through a gas-filled pipe. These thermoacoustic oscillations can greatly enhance the heat losses over those predicted by pure conduction theory. The Lockheed-Huntsville Thermoacoustic Oscillations (TAO) computer program has been modified for use in this study. In addition, a computer program for performing a power spectral density (PSD) analysis is being utilized.

Progress during this quarterly period is summarized in the following categories: (1) statistical analysis; (2) TAO parametric study; and (3) power spectral density calculations.

Statistical Analysis: The primary objectives of this statistical study is to determine the predominant amplitudes and frequencies of the thermal acoustic oscillations. The analysis involves first the determination of statistical parameters such as mean value, variance and standard deviation of the dependent variables (i.e., pressure, temperature, density and velocity profiles). In addition, several important statistical functions are determined and analyzed. These include the auto-correlation function, the power spectral density function, the cross-correlation function, and the cross spectral density function. The following is a brief discussion of the definitions and significances of the statistical parameters and functions (Ref. 1).

We start with a time series $x(t)$ having oscillatory properties and being valid a sufficiently long period $0 \leq t \leq T$. The series $x(t)$ may represent the calculated pressure, temperature, density or velocity solutions of the thermal acoustic oscillations computer program. The statistical parameters of $x(t)$, namely, the mean value $\bar{x}$, the variance σ_x^2, the mean square value ψ_x^2, and the standard deviation σ_x, are defined as follows:

$$\bar{x} = \frac{1}{T}\int_0^T x(t)\ dt \tag{1}$$

$$\sigma_x^2 = \frac{1}{T}\int_0^T \left[x(t) - \bar{x}\right]^2 dt \tag{2}$$

$$\psi_x^2 = \frac{1}{T}\int_0^T x^2(t)\ dt \tag{3}$$

$$\sigma_x = \sqrt{\sigma_x^2} \tag{4}$$

The mean value is simply the average of all values within the time interval of $0 \leq t \leq T$. The variance is the mean square value about the mean. The variance is a dynamic or fluctuating component of the time series. It is a measure of the degree of fluctuation. The mean square value represents the general intensity of the time series. It is the average of the squared value of the time history. The standard deviation is simply defined as the positive root of the variance.

By expanding Eq. (2), it can be shown that the variance is equal to the mean square value minus the square of the mean value. That is,

$$\sigma_x^2 = \psi_x^2 - \bar{x}^2 \tag{5}$$

Auto-Correlation Function: The auto-correlation function of an oscillatory time series $x(t)$ describes the general dependence of the values of x at one time or the value at another time. Consider a time history record $x(t)$ illustrated in Fig. 2. An estimate for the auto-correlation between the values of $x(t)$ at times t and $t+\tau$ may be obtained by taking the product of the two values and averaging over the observation time t. The observation time t is supposed to be sufficiently large to cover many times the periods of the waves contained in $x(t)$. In equation form, the auto-correlation function, $R_x(\tau)$, is defined as

$$R_x(\tau) = \frac{1}{T}\int_0^T x(t)\ x(t+\tau)\ dt \tag{6}$$

The quantity $R_x(\tau)$ is always a real-valued even function with a maximum at $\tau = 0$, and may be either positive or negative. In terms of the auto-correlation function, the mean value of $x(t)$ is given by

$$x = \left[R_x(\infty)\right]^{1/2} \tag{7}$$

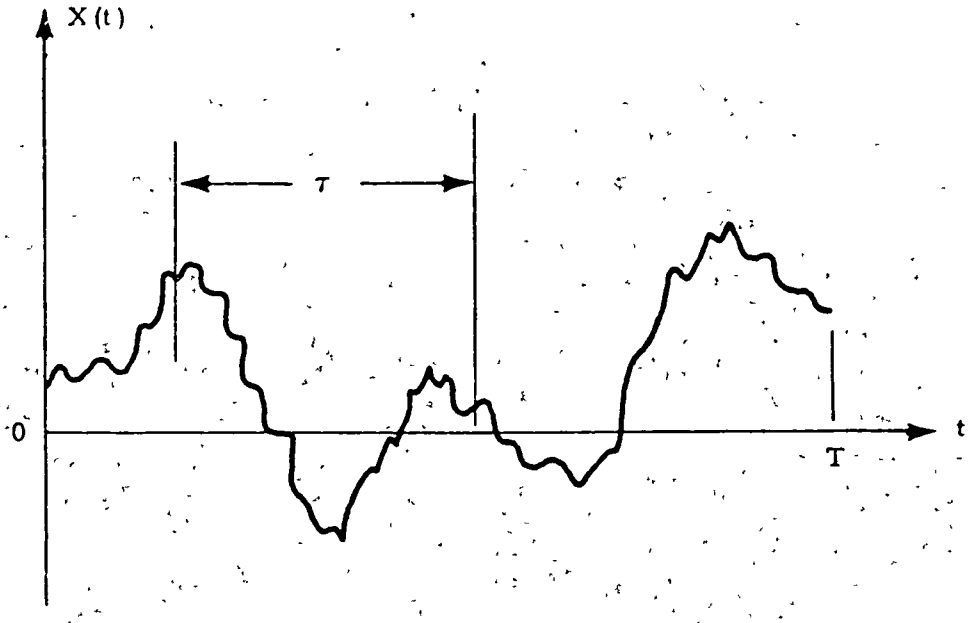

Fig. 2 - Auto-Correlation Measurement

In words, the mean value of x(t) is equal to the positive square root of the auto-correlation as the time displacement becomes very long. Similarly, the mean square value of x(t) is given by

$$\psi_x^2 = R_x(0) \tag{8}$$

That is, the mean square value is equal to the auto-correlation at zero time displacement.

Power Spectral Density Function: The power spectral density function (also called the auto-spectral density function) of x(t) describes the general frequency composition of x(t) in terms of the spectral density of its mean square value. The mean square values of the time series x(t) in a frequency range between f and $f + \Delta f$, i.e., $x(t, f, \Delta f)$, may be obtained by filtering the series with a band-pass filter having sharp cutoff characteristics, and computing the average of the squared output from the filter. This average squared value will approach an exact mean square value as the observation time, t, becomes large. That is, for sufficiently large t,

$$\psi_x^2(f, \Delta f) = \frac{1}{T}\int_0^T x^2(t, f, \Delta f)\, dt \tag{9}$$

Where $\psi_x^2(f, \Delta f)$ is the mean square value of x in the frequency range from f to $f + \Delta f$.

The power spectral density function of x(t) is defined as

$$G_x(f) = \lim_{\Delta f \to 0} \frac{\psi_x^2(f, \Delta f)}{\Delta f}$$

$$= \lim_{\Delta f \to 0}\left[\frac{1}{\Delta f}\cdot\frac{1}{T}\int_0^T x^2(t, f, \Delta f)\right]dt \tag{10}$$

Hence, the power spectral density of x(t) at the frequency f, i.e., $G_x(f)$, is the mean square value of x(t) at f per unit frequency.

An important property of the power spectral density function lies in its relationship to the auto-correlation function, $R_x(t)$. For a set of stationary oscillatory data, the two set statistical functions $G_x(f)$ and $R_x(t)$ are related by a Fourier transform as follows

$$G_x(f) = 2\int_{-\infty}^{\infty} R_x(t)\, e^{-j2\pi f t}$$

$$= 4\int_{0}^{\infty} R_x(t) \cos 2\pi f t \, dt \qquad (11)$$

Where $j = \sqrt{-1}$.

Other statistical properties of x(t), such as mean value and square value, are also related to $G_x(f)$.

A typical plot of power spectral density function versus frequency is shown in Fig. 3. The figure shows that the original time series x(t) contains two predominant waves of frequencies f_1 and f_2.

The principal application for a power spectral density function measurement of physical data is to establish the frequency composition of the data which, in turn, bears important relationships to the basic characteristics of the physical system involved. For our present study of thermal acoustic oscillations, a power spectral density analysis of the analytical results of pressure, temperature, etc., will enable us to determine the predominant frequency or frequencies of the system.

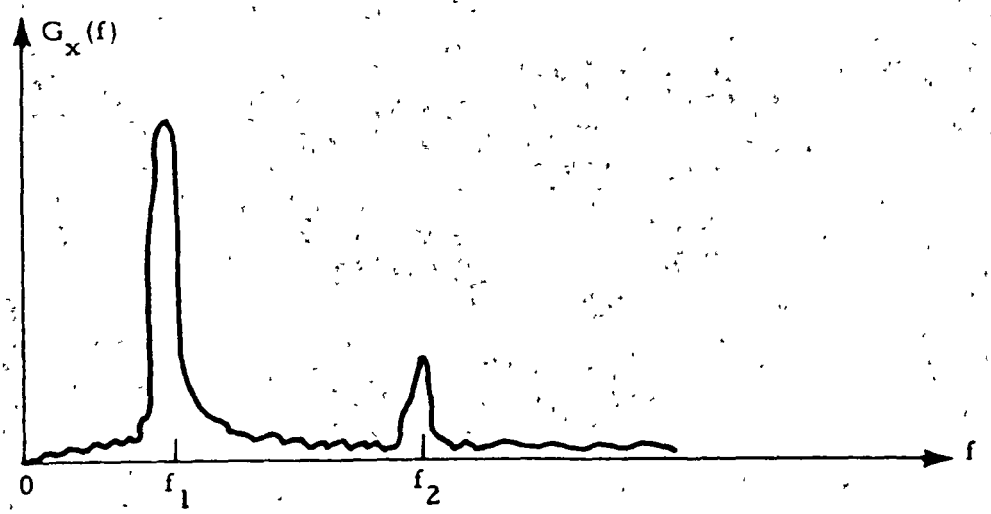

Fig. 3 - Power Spectral Density Plot

TAO Parametric Study: Computer runs which are being made consist of two types: (1) fixed length-to-diameter (L/D) tubes with parametric acoustic Reynolds number for use in constructing an existence diagram, and (2) generating data tapes with complete flow fields versus time for use in the PSD program. Two curves of particular interest are presented in Figs. 4 and 5. These are plots of temperature and pressure versus time for an open tube with L/D = 300. These are shown to illustrate the significance and need for a PSD analysis. Note that both profiles show a sequence of "high-frequency" waves superimposed on a "lower frequency" wave. The PSD analysis will operate on this type of data to extract the dominant frequencies of the waves. The temperature plot is shown at z = 0.5 (near warm end) and the pressure plot is shown at z = 0.95 (near cold end) which illustrates that this multi-wave characteristic is present at both ends of the tube.

One of the primary objectives of this study is to determine conditions which produce thermal acoustic oscillations. This result is being sought by performing a parametric analysis using the TAO program.

The parameters being studied are those given by Von Hoffmann et al. (Ref. 2): (1) ratio of hot to cold temperature (T_h/T_c); (2) length-to-diameter ratio of tube, L/D; (3) acoustic Reynolds number, Re; and (4) ratio of total tube length to cold part length, L/L_c. Figure 6 is a reproduction of the Von Hoffmann figure with TAO cases shown for comparison. Several other TAO cases are being run in order to construct a curve similar to that of Von Hoffmann. The data points shown are in reasonable agreement but with several apparent discrepancies. For example, at $T_h/T_c = 10$, the TAO solution shows that oscillations occur for values of the dimensionless parameter $\Delta = 100$ while Von Hoffman shows no oscillations above $\Delta = 30$. This is most likely due to the nonlinear effects included in the TAO solution while Von Hoffman's analysis is based on linearized equations.

The solid line indicates the trend of the curve for defining the existence criteria for thermal acoustic oscillations. Several other cases are being processed to refine this curve. This portion of the study will be completed during the November-December period.

Power Spectral Density Calculations: The Lockheed-Huntsville Statistical Analysis Computer Program is being utilized in this study. This program is a multi-function generation program for statistical analysis, i.e., it computes more than just the spectral density function.

The inputs x, y can be any functions of time such as temperature and pressure. These are supplied via magnetic tape from the TAO solutions. The program then calculates mean values, mean squared values, standard deviations and variances. The data are then detrended and tapered to give zero mean value and slope. The Fourier transform of the complex function z = x + jy is now computed using a Fast Fourier Transform (FFT) algorithm. The first calculations are then made for a number of statistical functions. The PSD function is of primary interest here but the cross correlations may prove useful also.

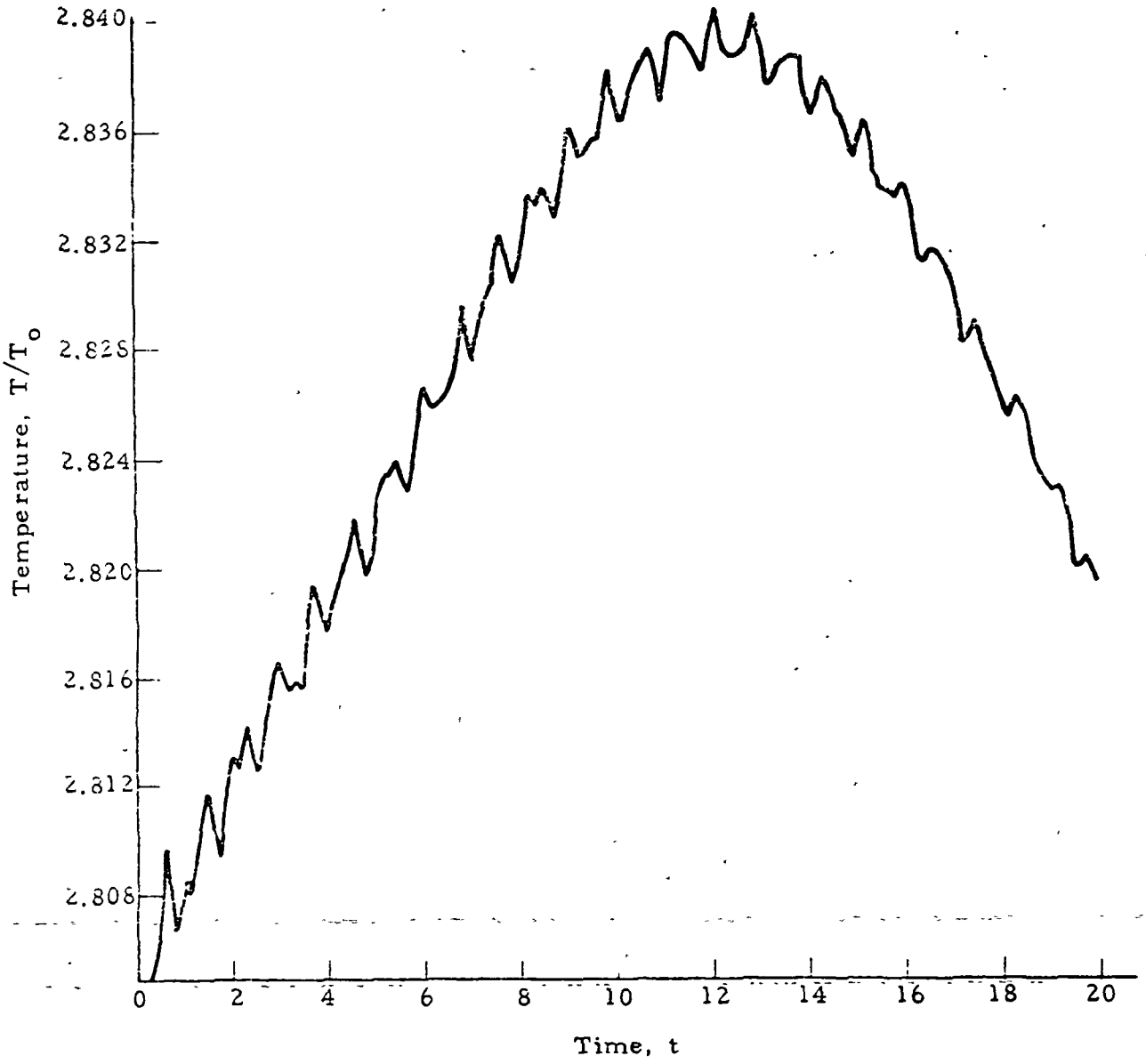

Fig. 4 - Temperature Profile at Z = 0.5 for Open Tube with L/D = 300

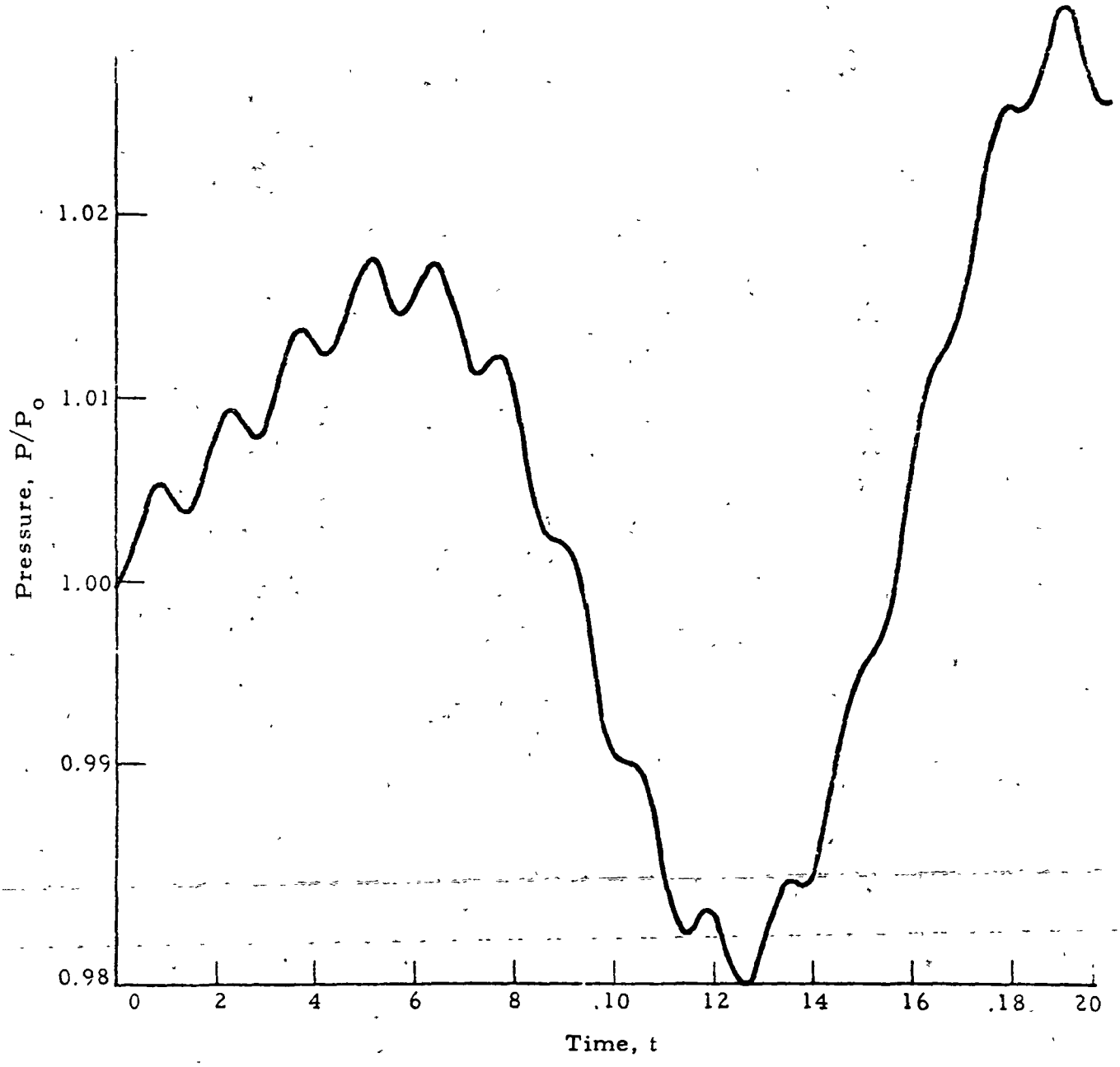

Fig. 5 - Pressure Profile at Z = 0.95 for Open Tube with L/D = 300

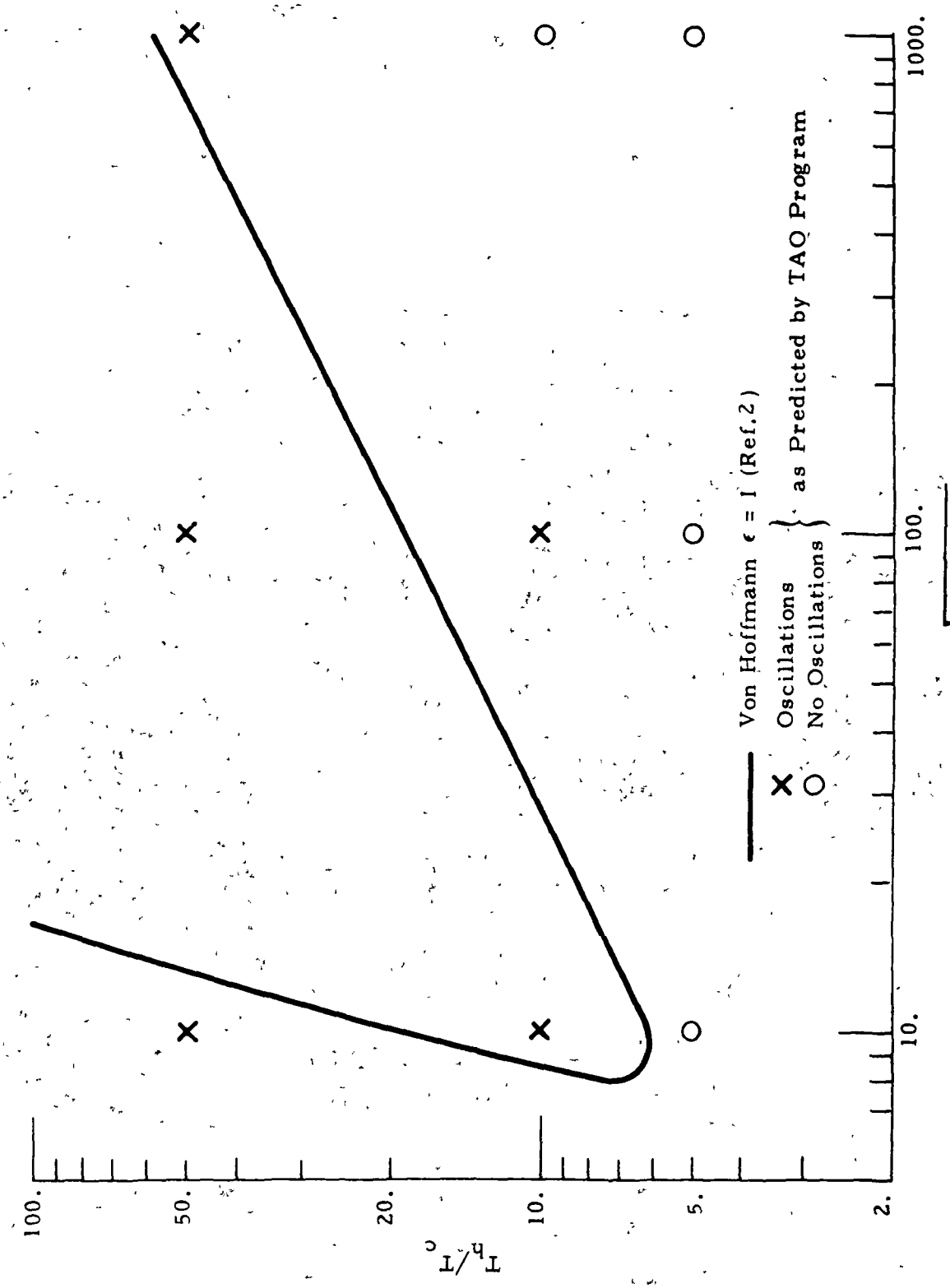

Fig. 6 - Preliminary Results for Parametric Study of Existence of Thermal Acoustic Oscillations

The program is operational for the general cases of inputting the x(t) via cards. Due to the complexities and large amounts of TAO data, the program has been modified to read the TAO solutions via magnetic tape.

During this performance period, the PSD program was run for several cases. The objective of these test runs was to verify the operation of the code modifications. The first test case consists of two square wave signals as shown in Fig. 7. The power spectral density function corresponding to the input signals is shown in Fig. 8. This basic checkout proved successful.

The next checkout case consists of a portion of temperature and pressure wave calculations from the TAO program. The input signals are given in Fig. 9. The top curve is temperature and the lower one is pressure (dimensionless). Figure 10 shows the calculated power spectral density. The pressure input here is a portion of a pure sine wave and thus the power spectral density shows a "spike" at the one frequency and zero elsewhere. This is correct for a pure sine wave. The temperature PSD plot shows the content decreasing at high frequencies. This is again the proper behavior.

A third case has been processed which consists of a larger portion of an actual TAO solution. Figure 11 shows the temperature (top) and pressure (bottom) input signals. Figure 12 is the corresponding power spectral density plot. This case appears to be correct, but further analysis is being done to verify the proper operation for this case. When this is finished, the TAO tapes for various L/D ratios will be run. These will be presented in the next progress report.

- Thermal Acoustic Oscillations Experimental Verification Program

The experimental verification program for the thermal acoustic oscillations analytical predictions has been prepared for initiation. In order that a more permanent form of experimental data may be obtained than would have been possible using an oscilloscope/camera system, an FM recorder will be used to obtain a permanent record of the frequency/amplitude output of the pressure transducer. This will enable repeat playbacks of the data and will also allow an analog-to-digital data translation for input to the power spectral density program if time allows. This portion of the program is desirable although not mandatory. The added capability will enhance the interpretation of the data if it is possible to input the experimental data into the PSD program.

The initial quantity of liquid helium to conduct the tests has been ordered, and testing is scheduled to begin within two weeks. The 0.95 cm outside diameter tube has been selected as the "control" tube, and will be tested over a range of $50 \leq L/D \leq 300$. Both stainless steel and aluminum tubes are to be tested. The complete test matrix of tubes and their characteristics are shown in Table 1.

- Long Term Cryogenic Storage Techniques

The basic system configurations for long term storage of liquid cryogen for a low-g environment have been selected. These configurations fall basically into four categories listed in Table 2.

Table 1

TAO EXPERIMENTAL VERIFICATION PROGRAM
TEST TUBING SIZES

Tube i.d. (cm)	Wall Thickness (cm)	Tube o.d. (cm)	L/D (-)	L (cm)
Stainless Steel Tubes				
0.30	0.089	0.478	150	45
0.658	0.147	0.953	50, 75, 100, 150, 300	33, 49.5, 66.1, 98.8, 197.6
1.297	0.305	1.905	30, 150	38.8, 194.3
Aluminum Tubes				
0.658	0.147	0.953	50, 100, 150	33, 66.1, 98.8

Table 2

SUMMARY OF CONFIGURATION CONCEPTS	
Configuration 1	Single blanket of MLI
Configuration 2	MLI with vapor cooled shield
Configuration 3	MLI with solid cryogen shroud
.3'	Solid hydrogen shroud
.3''	Solid nitrogen shroud
.3'''	Solid argon shroud
Configuration 4	MLI with radiator cooled fin

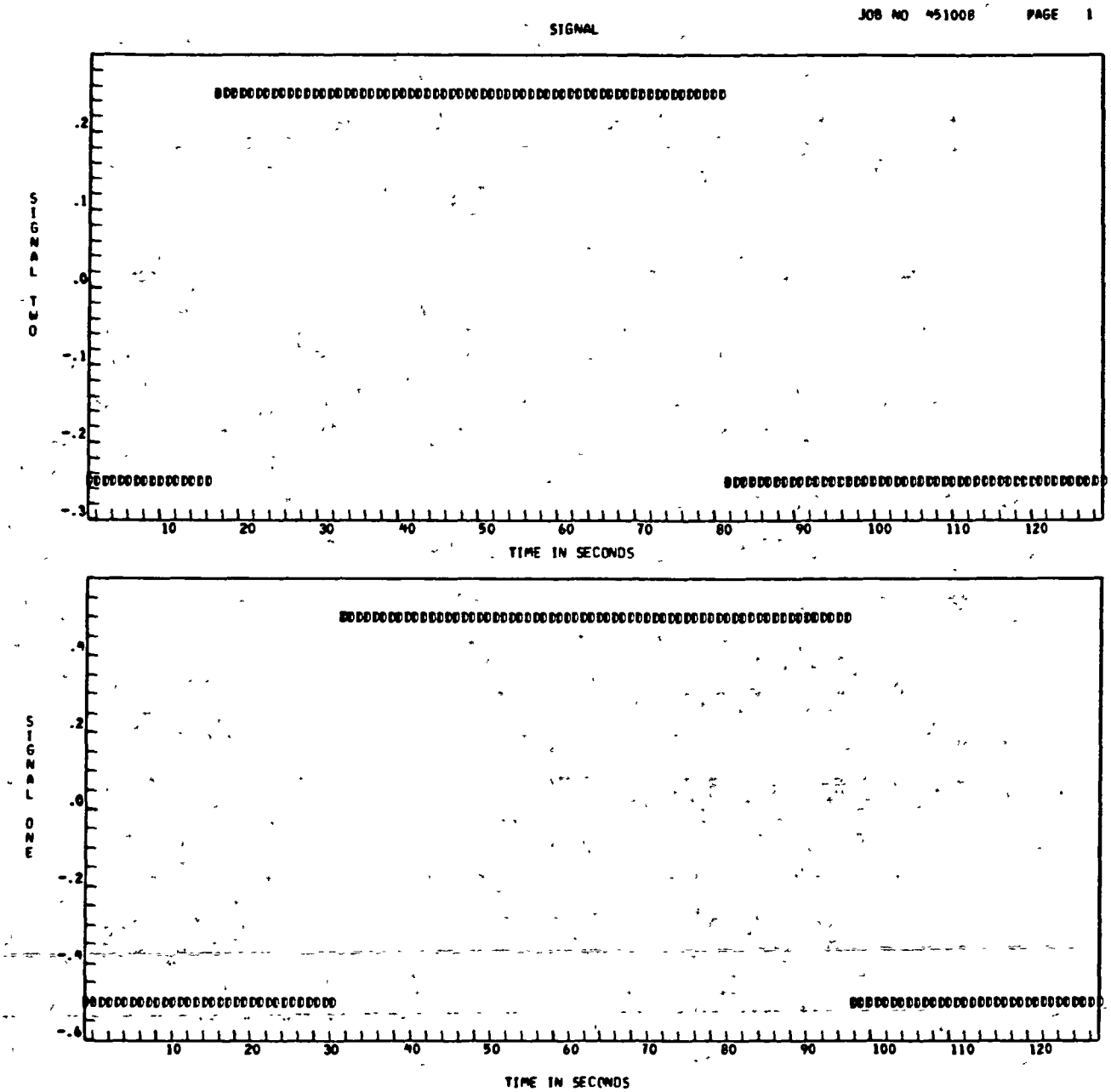

Fig 7 - Input Signal for PSD Checkout Run: Case 1

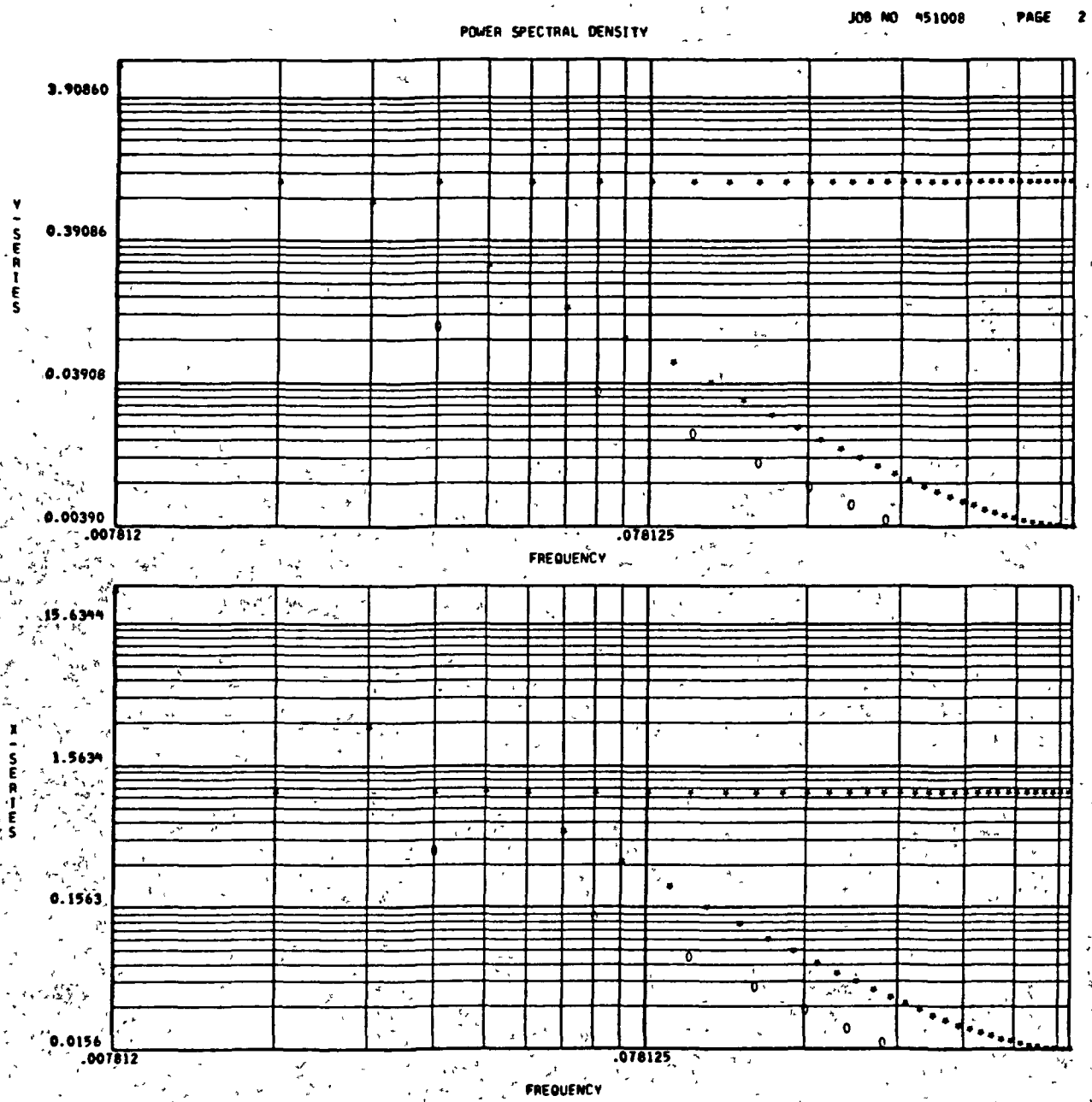

Fig. 8 - Power Spectral Density for Square Wave Input
(* = PSD Function, 0 = Smoothed Values)

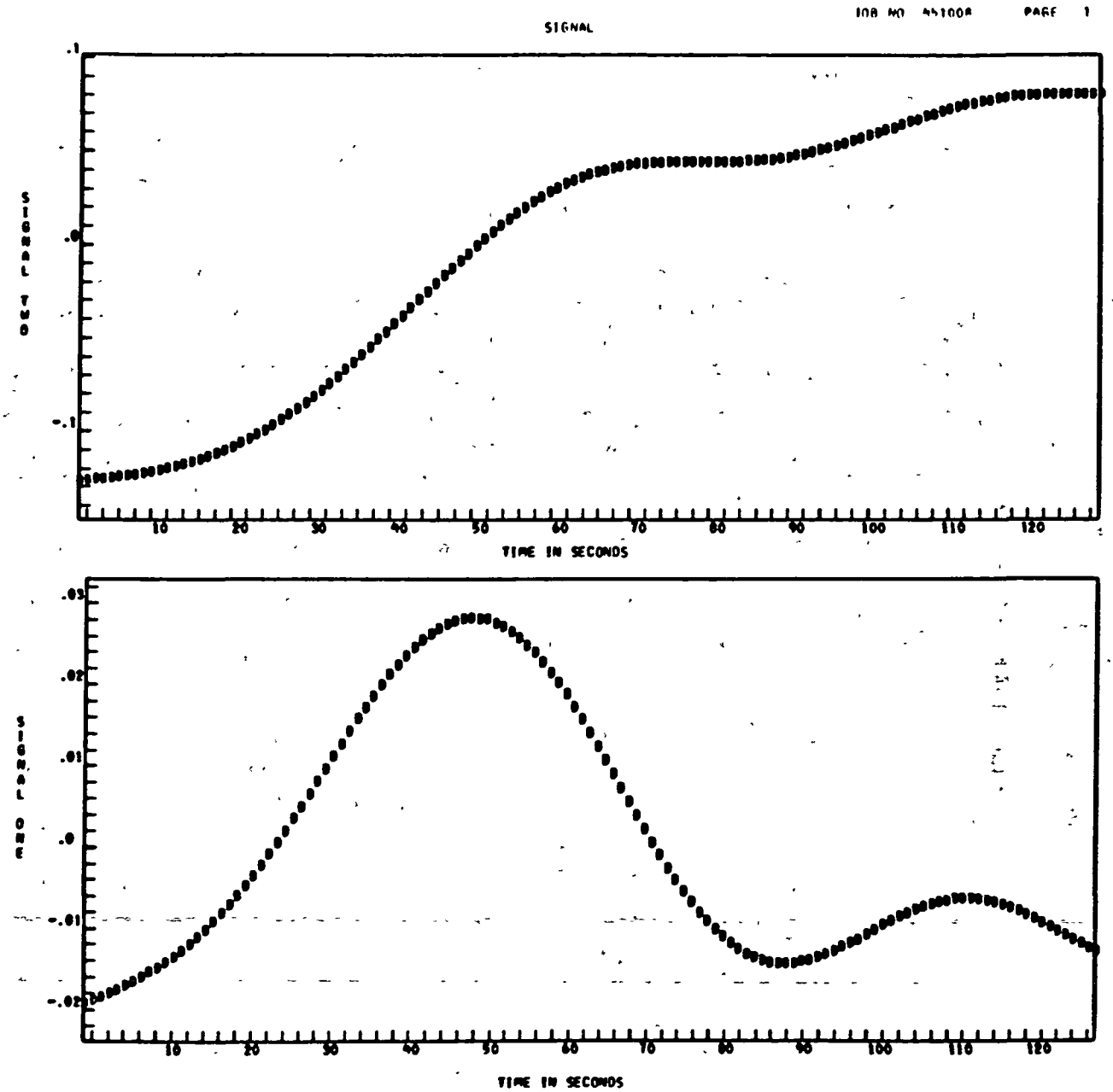

Fig. 9 - TAO Sample Inputs for PSD Program: Case 2

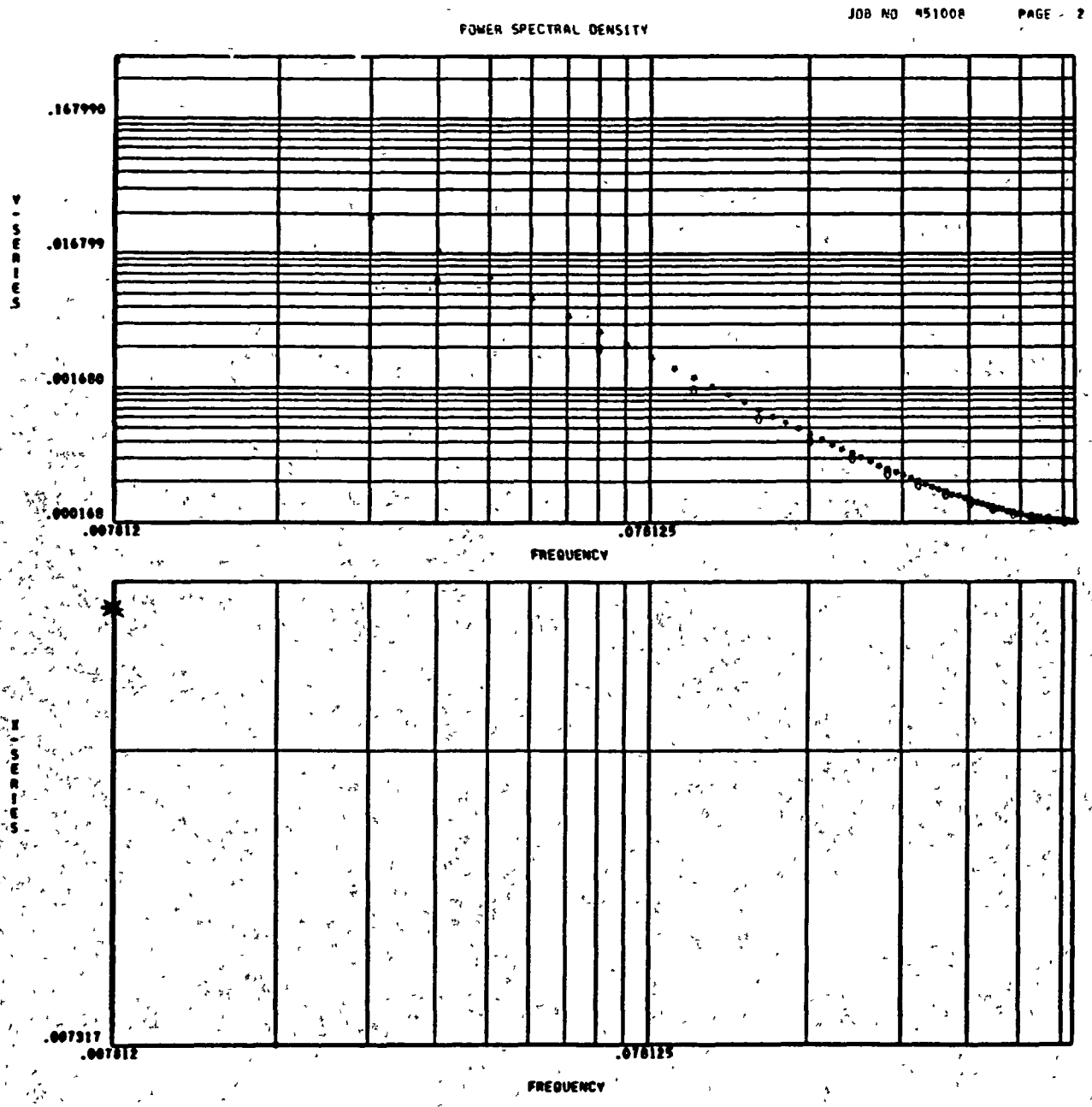

Fig 10 - Power Spectral Density for Sample TAO Inputs: Case 2
(* = PSD Function, 0 = Smoothed Value)

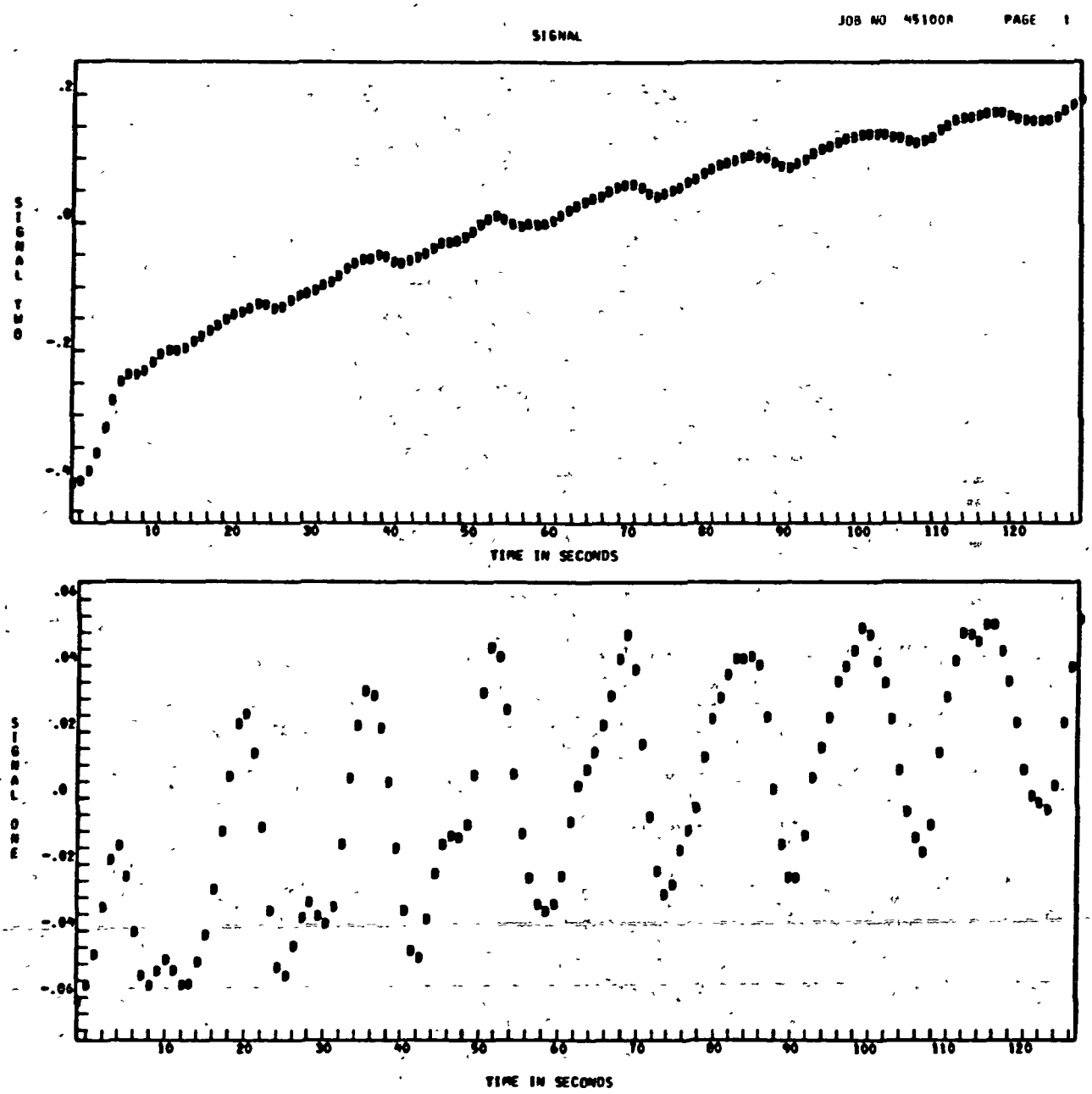

Fig. 11 - TAO Input for PSD Program: Case 3

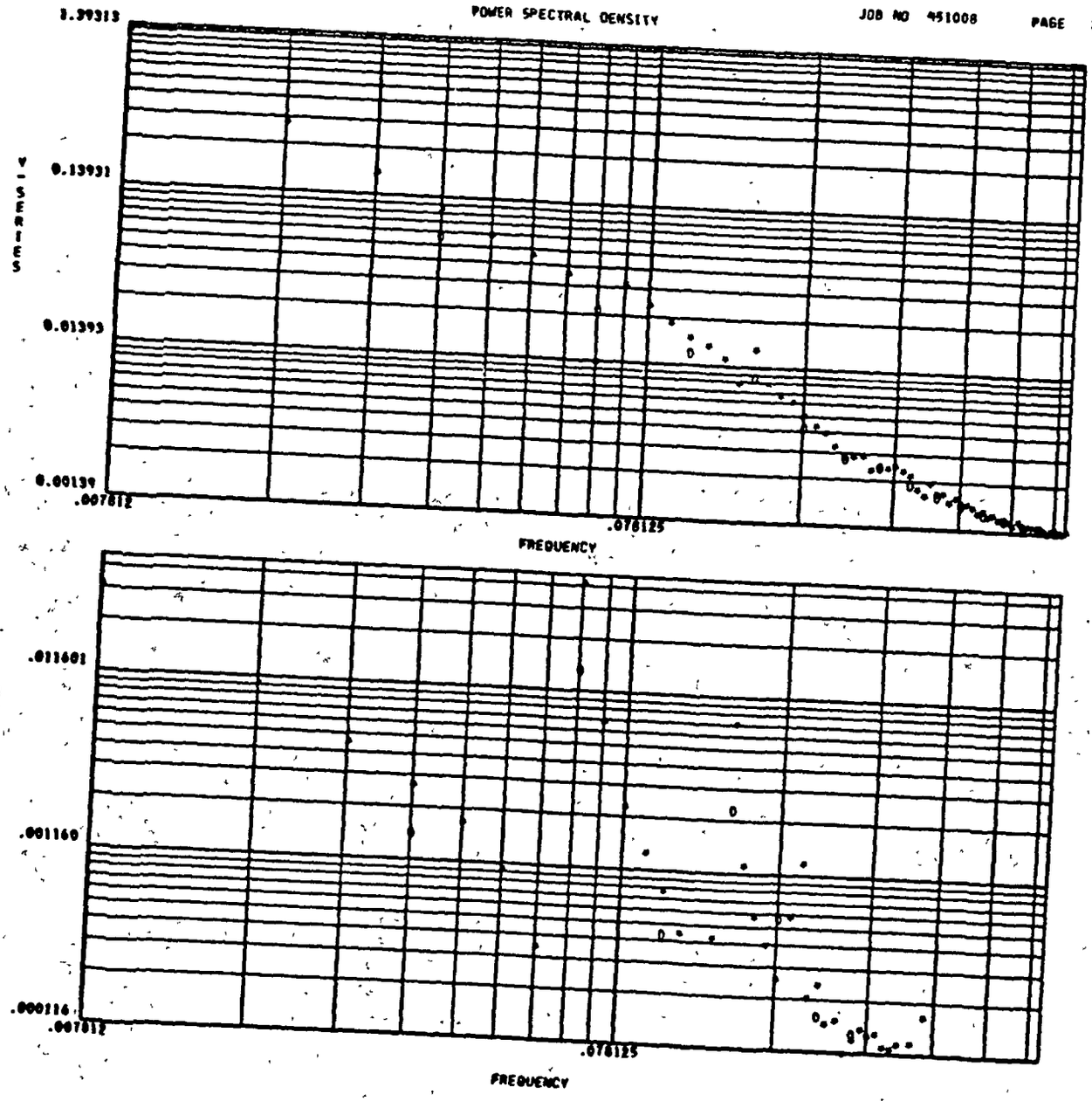

Fig. 12 - Power Spectral Density for TAO Case 3

Mathematical Models: The analytical models for these configurations are based on one-dimensional heat transfer through a homogeneous medium. There are two implications due to this basic simplification that are common to all configurations, namely:

- The cryogen tank wall is fully wetted
- There exist no property or temperature gradients orthogonal to a radius.

The latter implication impacts the modeling of such phenomena as penetration heat leaks, the heat transfer process in vapor cooled shields (Configuration 2), and the shorting of penetration heat loads at shields and cryogen shrouds (Configurations 2, 3 and 4) as will now be discussed.

Penetration Heat Leaks: The accompanying sketch (Fig. 13) indicates the method in which the penetration heat leaks to the liquid helium through support structures, vent tubes, electrical leads, and/or through the structure of the experiment itself will be modeled. The penetration load is the result of conduction heat transfer to the stored cryogen through several channels which are in parallel. In the absence of heat shorts to vapor cooled shields or solid cryogen cooled shrouds, these heat penetrations through the parallel channels will be subjected to the same temperature difference, $(T_{cry}-T_{amb})$. In order to vary the penetration heat load in a consistent manner, a range of values will be assigned to a "penetration conductance." The conductance must characterize the heat penetrations through all penetration channels and will therefore represent a summation of the conductances through all channels. Thus,

$$\overline{C} = \sum_{i=1}^{i_c} \frac{AK}{L}$$

i_c = number of penetration channels (supports, vents, loads, etc.)

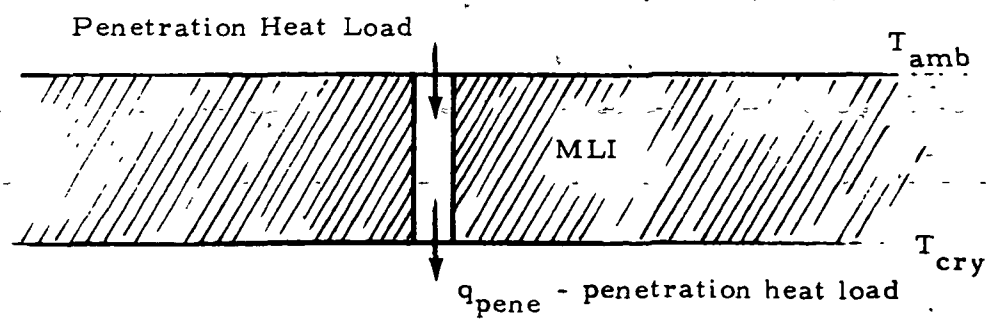

Fig. 13 - Model for Penetration Heat Load

The penetration conductance is determined by: (1) the geometry of the penetration channel which may be characterized by A/L (where A may be taken to be dependent on L and an appropriate average value for A may be defined); and (2) the thermal conductivity of the penetration channel which may be taken to be temperature dependent to arrive at an average value for K. The heat load due to a penetration will be accounted for by parameterizing thermal conductance for the penetration heat load such that the range of conductances for various support and vent schemes are covered. A designer may then estimate the penetration conductance of his cryostat in order to select the appropriate curve to be generated in this study.

A preliminary estimate for the range of penetration conductances was based on using 347 stainless steel and fiberglass supports. The size of the support members required to support cryostats weighing 45 kg and 227 kg for 10 g loadings with a safety factor of 2 were calculated. The lengths of the supports were taken to be 0.3 m and 1.55 m along the penetration channel. Table 3 summarizes the influence of support material and liftoff cryostat mass on the penetration conductance.

Table 3

ESTIMATE OF THERMAL CONDUCTANCE FOR SUPPORTS

Material	Yield Strength $kg\text{-}m^{-2}$	K-Temp. Averaged $W\text{-}m^{-1}\text{-}deg^{-1}$	Liftoff Mass = 45 kg L = 1.52 m $W\text{-}{}^{o}R^{-1}$	Liftoff Mass = 226 kg L = 0.30 m $W\text{-}{}^{o}R^{-1}$
347 Stainless Steel	9.0×10^{7}	12.6	0.47×10^{-4}	1.172×10^{-3}
Fiberglass	9.1×10^{6}	5.0	0.146×10^{-4}	0.366×10^{-3}

The conductances listed in Table 3 do not account for penetrations through electrical leads and vent tubes. One might double the conductances in Table 3 to account for these effects. Also, a cryostat may be designed for retractable supports once the vehicle is placed in orbit in which case the conductances in Table 3 would be larger than the long term conductance to the cryogen. To appropriately parameterize the conductances (see Table 5), it appears that conductances should cover a range from 10^{-3} to 10^{-7} $W/{}^{o}R$.

Vapor Cooled Shield Efficiency: Vapor cooled shields immersed within the MLI are designed to allow the boiloff vapor to intercept a portion of the heat leak through the MLI and penetration channels. This implies the presence of a lateral temperature gradient within the shield which is in opposition to the one-dimensional heat transfer assumption on which the math model is based. To circumvent this difficulty an efficiency is defined for the heat absorbed by the boiloff vapor during its residence within the shield. Since the

vapor cooled shield is essentially a heat exchanger, the efficiency of the shield is defined with the standard heat exchanger efficiency (see Fig. 14).

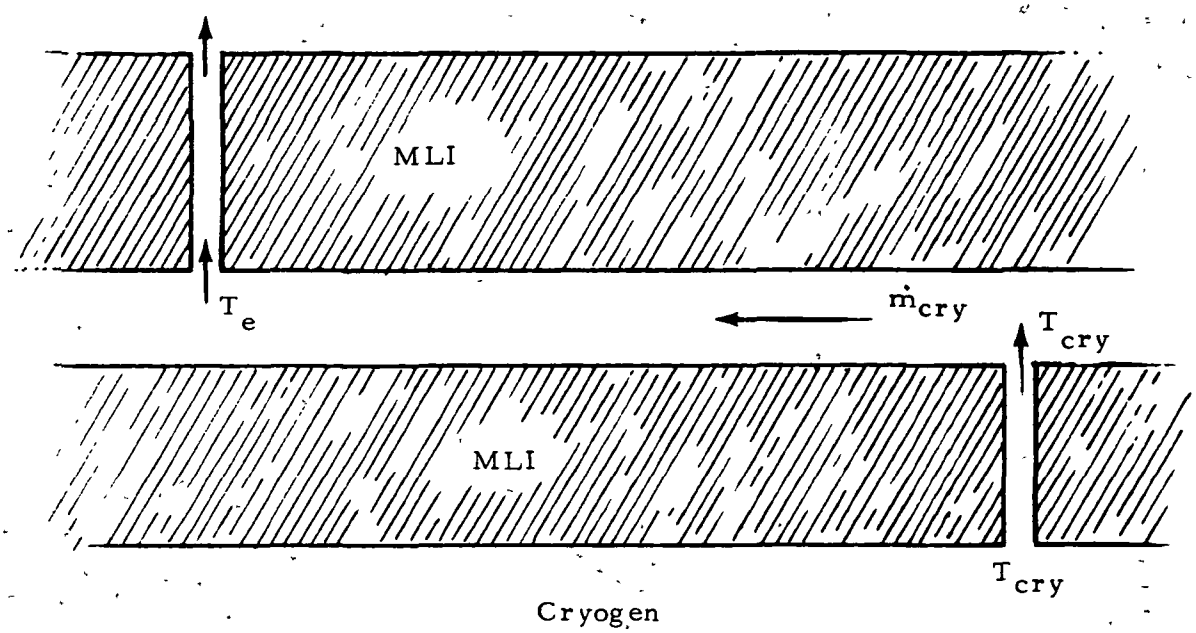

Fig. 14 - Schematic of Vapor Cooled Shield

The maximum heat is absorbed by the boiloff vapor if the vapor leaves at the temperature of the shield. In actual operation the vapor leaves at a temperature below that of the shield.

$$\eta_{V.S.} = \frac{q_{V.S._{actual}}}{q_{V.S._{ideal}}} = \frac{T_e - T_{cry}}{T_{sh} - T_{cry}}$$

$$q_{V.S.} = \eta_{V.S.} \dot{m}_{cry} C_{p_{cry}} (T_{sh} - T_{cry})$$

Thermal Short Efficiency: Efficient design of a cryostat often incorporates schemes for allowing vapor cooled shields and cryogen shrouds to absorb a portion of the penetration heat loads. This is referred to as thermal shorting

of the penetration heat load. The presence of a thermal short in a cryostat design violates the one-dimensional heat transfer assumption. To allow the inclusion of investigating the influence of thermal shorts in this analytical work, a definition for thermal short efficiency is made from which the magnitude of the thermal short may be determined. Reference should be made to Fig. 15. The maximum thermal short occurs if $T_p = T_{sh}$. In that case q_3 may be defined for equal AK/L between shield/environment and shield/cryogen as

$$q_3 = q_{ideal} = \frac{AK}{L} (T_{amb} + T_{cry} - 2\,T_{sh})$$

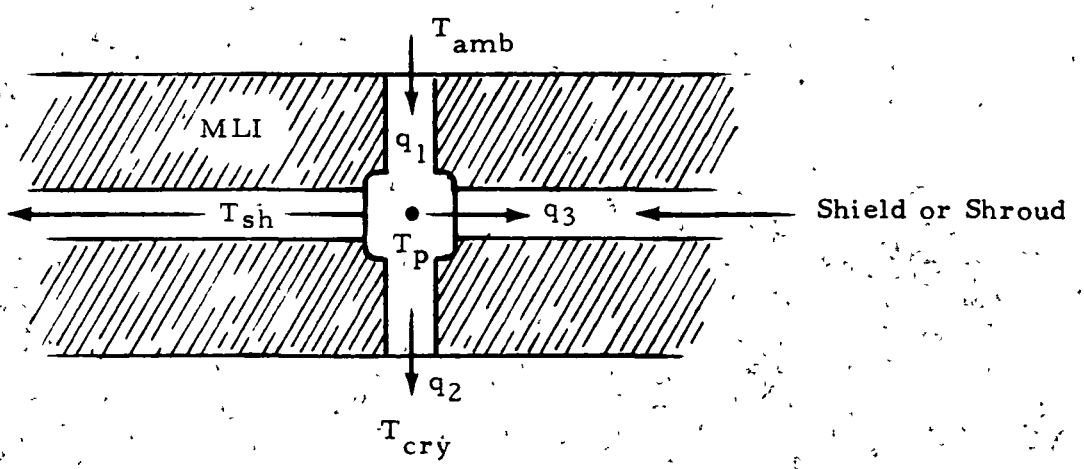

Fig. 15 - Schematic of Thermal Short

In actual operation T_p is above T_{sh} and q_3 is less than q_{ideal}. Thus, the thermal short efficiency is defined as the ratio of actual thermal short to the maximum attainable thermal short

$$\eta_{t.s.} = \frac{q_{actual}}{q_{ideal}}$$

from which T_p may be defined in terms of T_{amb}, T_{cry}, T_{sh} and $\eta_{t.s.}$ as

$$T_p = \frac{T_{amb} + T_{cry} - \eta_{t.s.}\,(T_{amb} + T_{cry} - 2\,T_{sh})}{2}$$

The penetration heat leak to the cryogen is then

$$q = -\frac{AK}{L}(T_{cry} - T_p)$$

and the magnitude of the thermal short is

$$q = \frac{AK}{L}(T_{amb} + T_{cry} - 2\,T_p)$$

It should be noted that the magnitude of the thermal conductance is taken to be constant throughout the penetration channels in the above definition of thermal short efficiency. This assumption is probably not too restrictive because previous studies of cryogen storage systems, particularly shield designs, indicate that the optimum shield spacing is roughly equidistant between environment and cryogen.

Configuration Equations: The equations used to describe a cylindrical cryogen tank with spherical end caps was presented in the last progress report. Briefly, the heat leak through the MLI was given by the equation:

$$q_{MLI} = 2\pi\left[\frac{2\,r_1\,r_2}{(r_2 - r_1)} + \frac{L}{\ell n(r_2/r_1)}\right]\int_{T_1}^{T_2} K_{MLI}\,dT$$

where r_1 and r_2, and T_1 and T_2 are the inside and outside cryostat radii and temperatures, respectively. K_{MLI} is the conductivity of the MLI perpendicular to its grain, and L is the length of the cylindrical section of the container.

The total heat load on the cryogen was given to be the sum of the heat leaks from the experiment, through the MLI, and through the penetrations. The heat absorbing capacity of the cryogen was calculated from the equation for the cryogen mass and its heat of vaporization which was assumed to be used uniformly over the storage time required of the cryostat. This heat absorbing capacity was then set equal to the total heat load and the equation solved for the cryogen mass. Finally a transcendental equation for r_2 as a function or r_1 was found by calculating the mass of the cryogen based on its density and storage volume, and then eliminating the cryogen mass by equating this equation with the above described equation. Once r_2 is found for a given r_1 the total system mass is calculated and stored. The value of r_1 is then incremented, the value of r_2 is again determined and the resulting total system mass is compared with that previously calculated. This procedure is repeated until the minimum total system mass is calculated, at which time the minimum total system mass and the corresponding parameters are output. Figures 16 through 19 show results obtained from the computer program using these

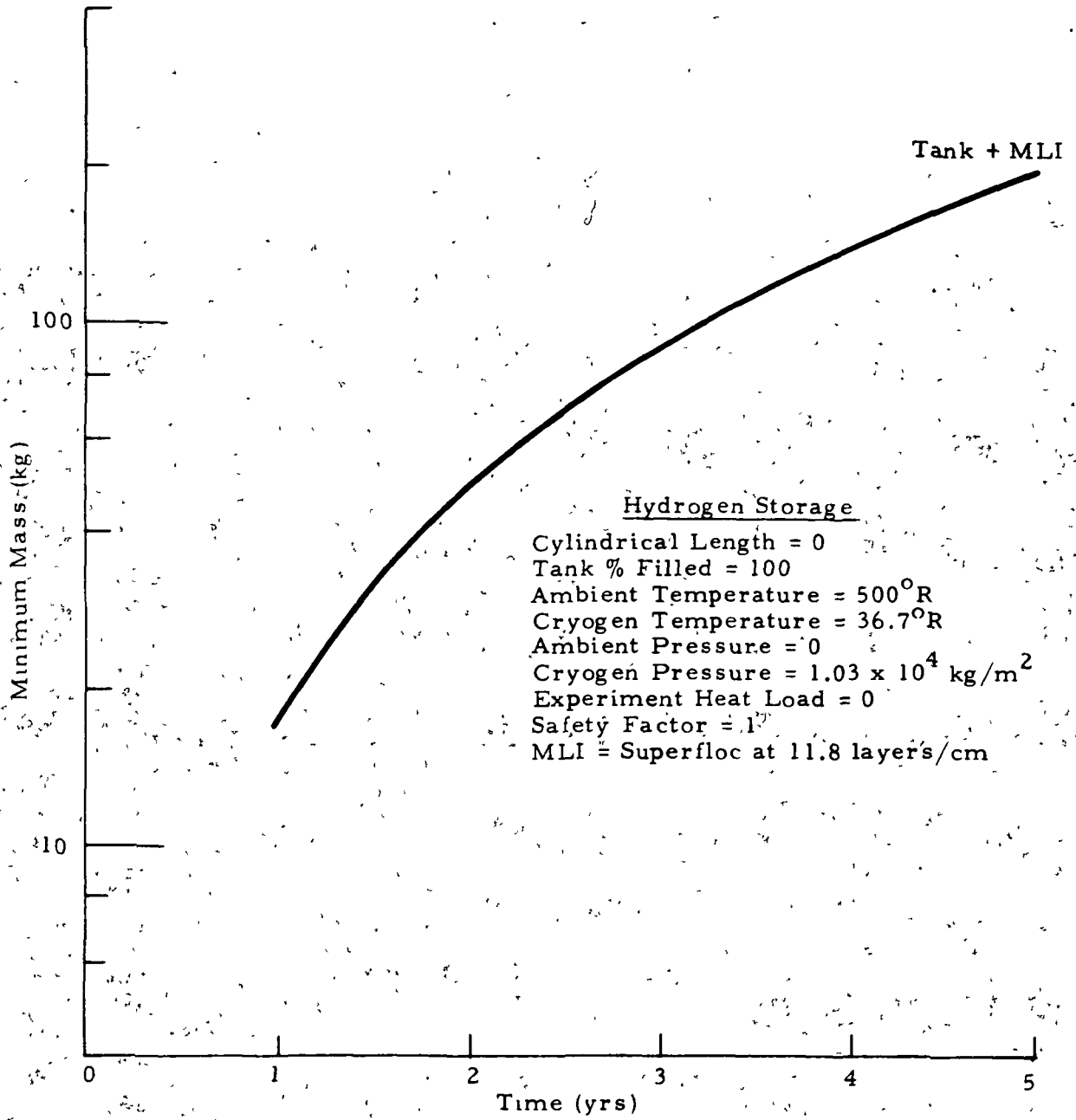

Fig. 16 - Minimum Total System Mass for Hydrogen as a Function of Storage Time for Configuration 1

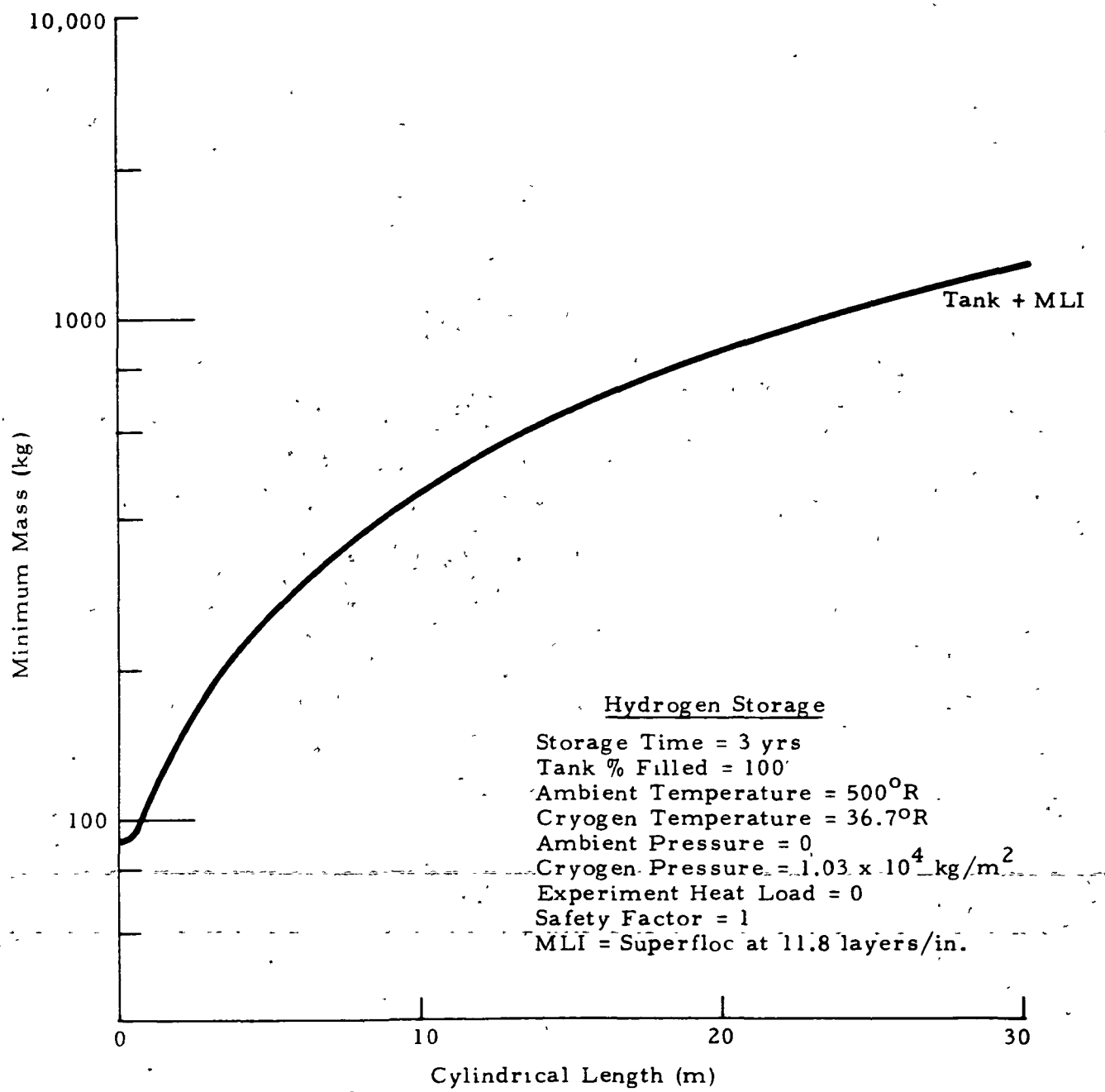

Fig. 17 - Minimum Total System Mass for Hydrogen as a Function of the Length of the Cylindrical Section of the System for Configuration 1

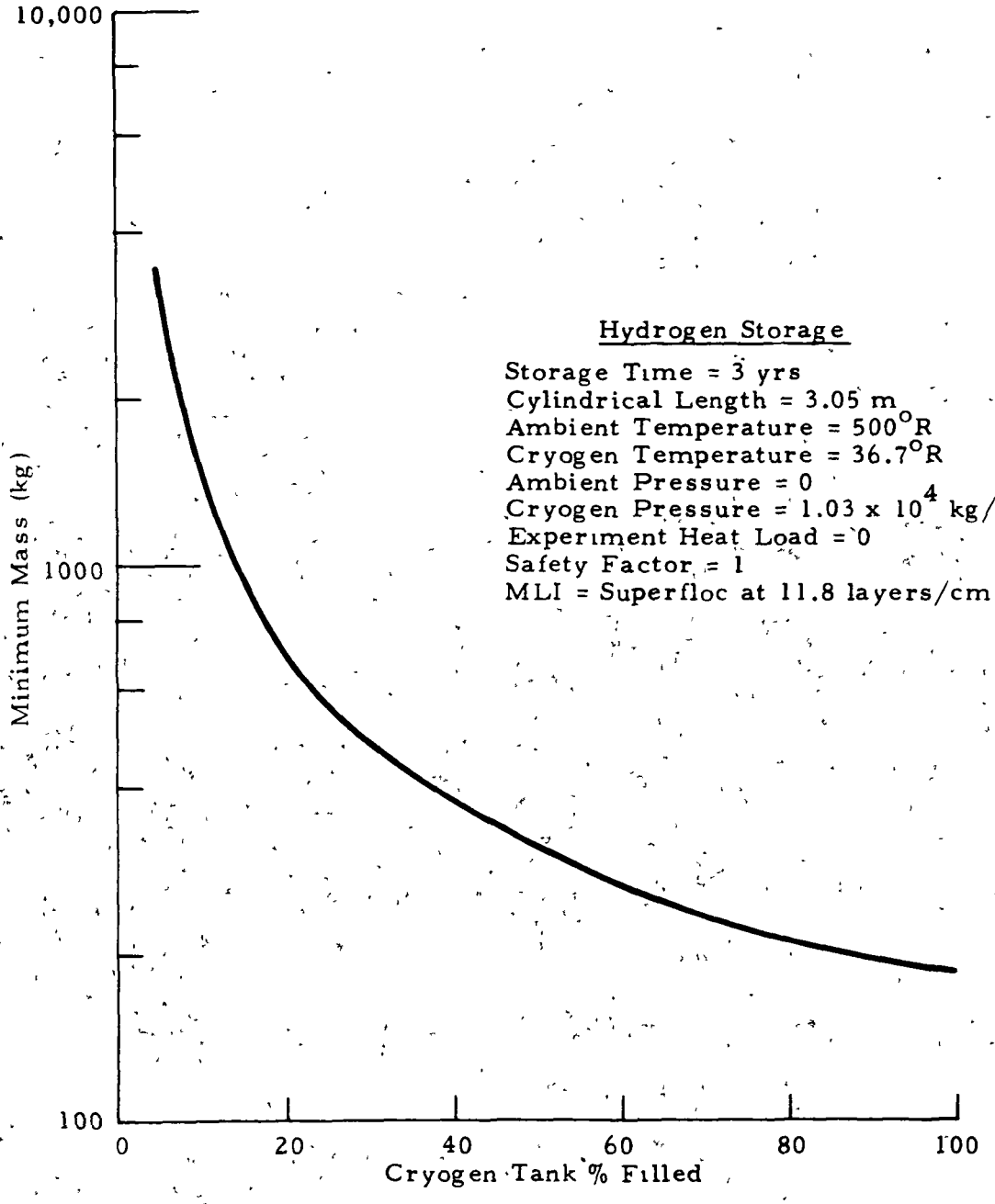

Fig. 18 - Minimum Total System Mass for Hydrogen as a Function of the Percent Fill of the Cryogen Tank for Configuration 1

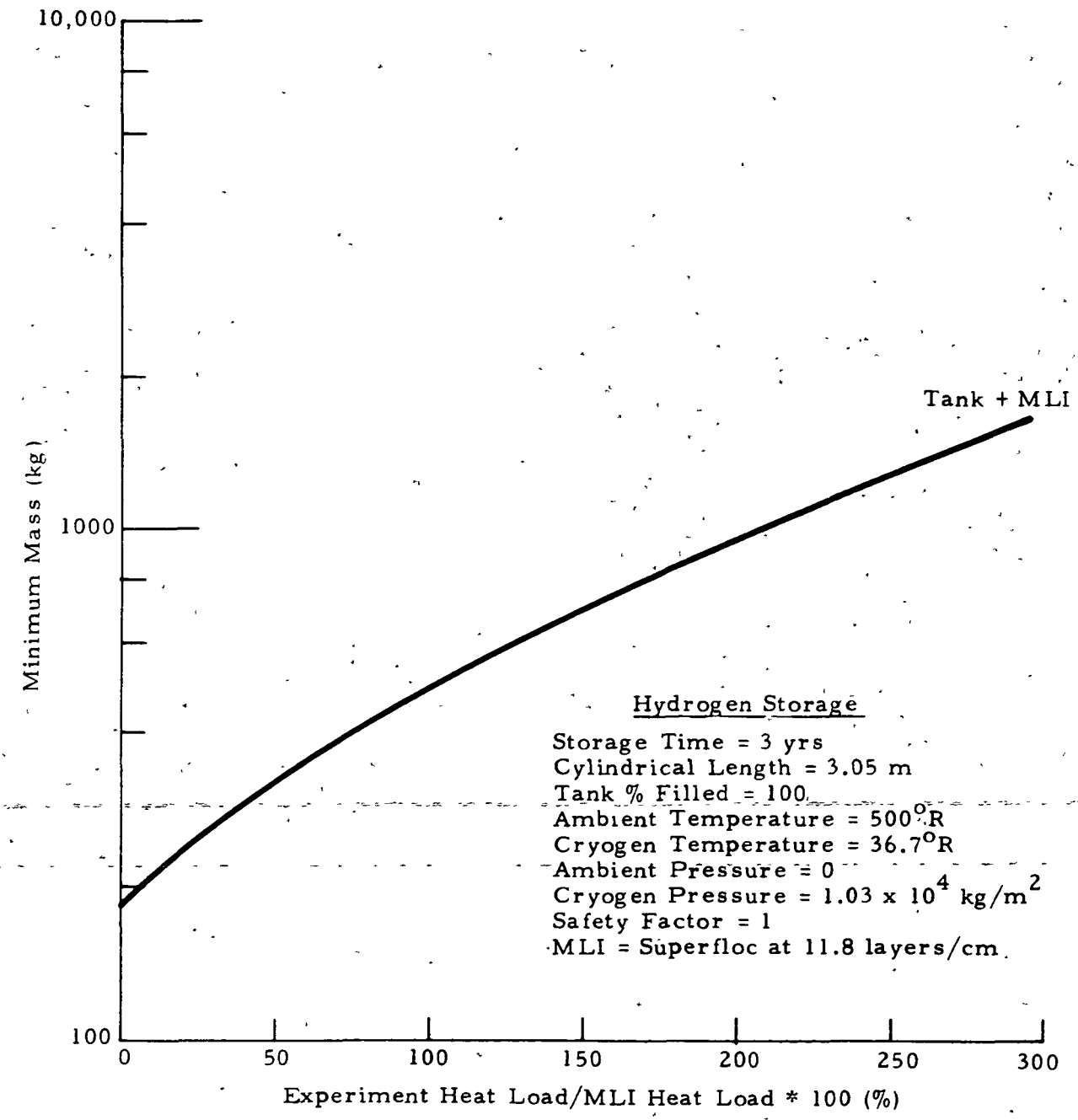

Fig. 19 - Minimum Total System Mass for Hydrogen as a Function of the Experiment Heat Load for Configuration 1

equations and procedure. The figures show the effect of storage time, length of cylindrical section, the percent which the cryogen tank is filled, and the experiment heat load on the minimum total system mass when hydrogen is stored using Configuration 1. The associated parameters are also shown on each figure. In particular, Fig. 16 shows the effect that the storage time requirements have on the minimum mass for a spherical configuration since the cylindrical length is zero. Doubling the storage time from one to two years will almost triple the minimum storage mass. Figure 17 shows the effect of varying the length of the cylindrical cryostat section on minimum total system mass for a storage time requirement of three years. Again zero cylindrical length would correspond to a spherical container. The cylindrical lengths are in meters and do not describe the particular shapes of the containers. An option will be installed in the computer program which will allow tank length-to-diameter ratios to be parameterized. Figure 18 shows the influence which the percentage of tank fill has on the total system mass for a container with a three-year storage requirement, and a length of 3.05 m. For this solution, there is assumed to be no net heat input by an experiment load. As expected, the figure shows the total system mass increasing very rapidly for percent tank fill approaching zero. Figure 19 shows the effect which the ratio of the experiment heat load and the MLI heat load has on the minimum total system mass, again for a storage time of three years and a cylindrical length of 3.05 m. The experiment mass and volume are neglected. For Configuration 1, the experiment heat load and the penetration heat loads can be treated exactly the same. Therefore, since the experiment mass and volume are neglected, this figure is even more appropriate for penetration heat leaks since the mass of the penetrations are normally small compared to the total system mass. For the figure, 0., 100., 200. and 300% penetration heat load corresponds to 0., 1, 2 and 3 times the MLI heat load, respectively.

Configuration 2 is similar geometrically with Configuration 1 except that Configuration 2 has a vapor cooled shield (VCS) embedded within the MLI, as is shown in Fig. 20. The method of solution of this configuration is to initialize r_1 and the VCS temperature (T_2) and use the equation described for Configuration 1 to calculate r_2 and the associated masses and heat fluxes. The rate of the cryogen vapor mass flow is calculated based on the initial mass of cryogen divided by the storage time, which assumes a steady state solution. The cooling capacity of the VCS can then be calculated based on the shield temperature and the cryogen temperature as:

$$q_{VCS} = \eta_{shield} \dot{m}_{\substack{cryo \\ vapor}} C_{p_{\substack{cryo \\ vapor}}} (T_{shield} - T_{cryo})$$

where η_{shield} is the heat transfer efficiency of the shield. The heat transferred from the outer radius to the VCS, r_3 to r_2, is then the heat transferred between the VCS and the cryogen tank, r_2 to r_1, plus the heat absorbed by the VCS, i.e.,

$$q_{2-3} = q_{1-2} + q_{VCS}$$

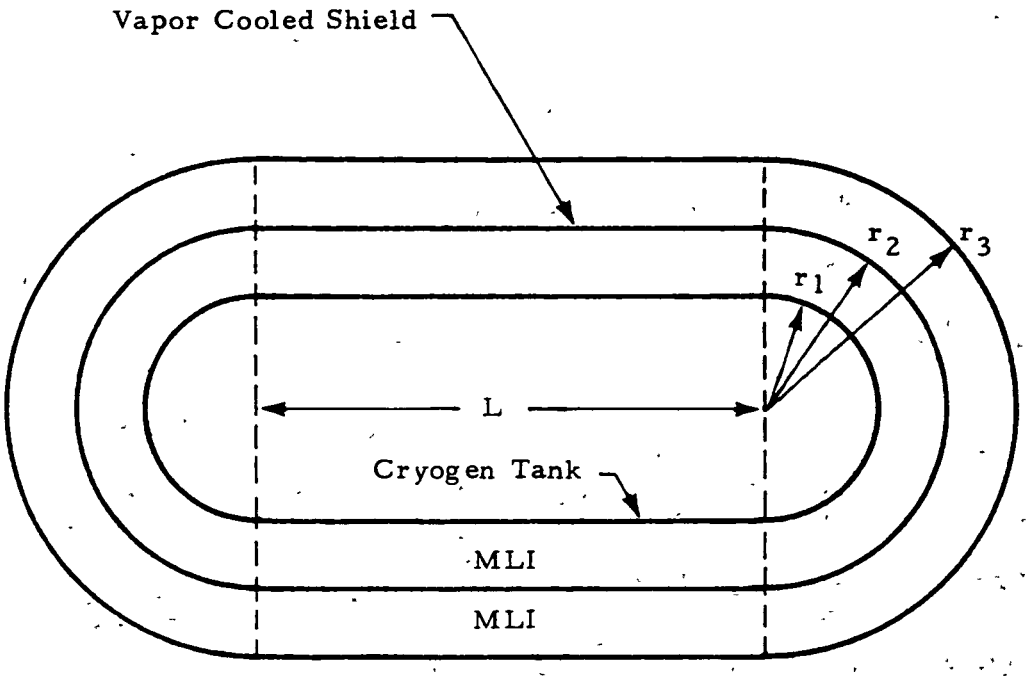

Fig. 20 - Geometry for Configuration 2

which must also be the same as the sum of the individual modes of heat transfer from r_3 to r_2, i.e.,

$$q_{2-3} = q_{MLI_{2-3}} + q_{pene_{2-3}}$$

where the calculation of $q_{pene_{2-3}}$ will be as described earlier. The heat transferred through the MLI from r_3 to r_2 is then

$$q_{MLI_{2-3}} = q_{1-2} + q_{VCS} - q_{pene_{2-3}}$$

Also, it is known that

$$q_{MLI_{2-3}} = 2\pi \left[\frac{2\, r_2\, r_3}{(r_3 - r_2)} + \frac{L}{\ell n (r_3/r_2)} \right] \int_{T_2}^{T_3} K_{MLI}\, dT$$

The prior two equations are then used to determine r_3. When r_3 is found for a particular VCS temperature, and after determining the mass of the vapor cooled shield from

$$M_{VCS} = 2\rho_{MAT} (4\pi r_2^2 + 2\pi r_2 L) \text{thick}_{wall}$$

the mass of MLI between r_2 and r_3 is calculated, and the total system mass is determined from

$$M_{total} = M_{Config.1} + M_{VCS} + M_{MLI_{2-3}} + M_{pene_{2-3}}$$

which is stored. The VCS temperature is incremented and the above procedure repeated until the minimum total system mass is determined. The above equations and procedure have been programmed into a computer routine which is in the final stages of development.

Summary of Assumptions Incorporated in Math Models: In order to construct a convenient set of parametric curves delineating the influence of configuration design on the mass of liquid helium systems, several simplifying assumptions have been made which, it is thought, do not severely compromise the validity of the mathematical models. These assumptions are summarized in Table 4 for the basic design configurations. The assumptions made for Configuration 1 are common to all configurations. Configurations 2, 3 and 4 require additional assumptions.

A preliminary matrix for the parametric study of liquid helium storage is shown in Table 5. The parameters considered to be most important are:

- Storage time
- Penetration conductance
- Experimental heat load
- Tank L/D

These variables have been given emphasis in both range of parameter variation and in number of computer runs in the analytical investigation of their influences on the minimum system mass required for liquid cryogen storage. The parameters that will be varied to a lesser extent are:

- Tank ullage (includes experimental volume)
- Vapor shield efficiency (applicable to Configuration 2)
- Thermal short efficiency (Configurations 2, 3 and 4)

Table 4

SUMMARY OF ASSUMPTIONS FOR PARAMETRIC STUDY

Configuration	Assumptions
1	One-dimensional heat transfer along radius • Cryostat wall is fully wetted • No localized boiling • No lateral temperature or property gradients in MLI Penetration conductance is constant Radial temperature gradient in tank wall is small Penetration channels are not vapor cooled Weight of supports, vents, electrical leads, and experiment are not considered in total system mass
2, 3, 4	Constant temperature shield, shroud, fin Penetration channels are cooled only at thermal shorts Penetration conductance is constant between external surface, shorts and cryogen

The following parameters will be fixed for analytical study:

- External surface temperature of cryostat: 530°R
- Liquid helium temperature: 5°R (saturated conditions)
- MLI: superfloc at 11.8 layer/cm
- Tank material: aluminum

Table 5

PRELIMINARY PARAMETRIC MATRIX FOR LIQUID CRYOGEN STORAGE STUDY

Configuration	Store Time	Pan Cond. (W/°R)	Test Load (W)	Tank L/R	Ullage (%)	$\eta_{V.S.}$ (%)	$\eta_{T.S.}$ (%)	Comments
1	0.25 0.5 1.0 2.0	10^{-3} 10^{-4} 10^{-5} 10^{-7}	1.5 0.3 0.03 0.003	0 1.0 2.0	5	–	–	Principal Matrix (192 runs)
1	0 25 0.5 1.0 2.0	10^{-5}	0.03	0	10 20 30	–	–	Delineate Influence of Ullage (12 runs)
2' One Shield	0.25 0.5 1.0 2.0	10^{-3} 10^{-4} 10^{-5} 10^{-7}	1.5 0.3 0.03 0.003	0 1.0 2.0	5	100	100	Principal Matrix (192 runs)
2'	0.25 1 0 2.0	10^{-5}	0.03	0	5	75 50	100	Delineate Influence of Shield Efficiency (6 runs)
2'	0.25 1.0 2.0	10^{-5}	0.03	0	5	100	90 80 50	Delineate Influence of Thermal Short Efficiency (9 runs)
3' H_2 Shroud at 20°R	0.25 0.5 1 0 2.0	10^{-3} 10^{-5} 10^{-7}	1.5 0.03 0.003	0 1 0	5	–	100	Principal Matrix (72 runs)
3'	0.25 1.0 2.0	10^{-5}	0 03	0	5	–	90 80 50	Delineate Influence of Thermal Short Efficiency (9 runs)
3'' N_2 Shroud at 100°R	0.25 0,5 1.0	10^{-3} 10^{-5} 10^{-7}	1 5 0.03 0.003	0 1.0	5	–	100	Principal Matrix (72 runs)
3''	0.25 1.0 2.0	10^{-5}	0.03	0	5	–	90 80 50	Influence of Thermal Short Efficiency (9 runs)
3''' – Argon Shroud at 100°R	0.25 0 5 1.0 2.0	10^{-3} 10^{-5} 10^{-7}	1.5 0.03 0.003	0 1.0	5	–	100	Principal Matrix (72 runs)
3'''	0.25 1.0 2.0	10^{-5}	0.03	0	5	–	90 80 50	Influence of Thermal Short Efficiency (9 runs)
4' Radiator Cooled Fin	0.25 0.5 1.0 2.0	10^{-3} 10^{-4} 10^{-5} 10^{-7}	1.5 0 3 0.03 0 003	0 1 0 2.0	5	–	100	Principal Matrix (192 runs)
4'	0.25 1.0 2.0	10^{-5}	0.03	0	5	–	90 80 50	Influence of Thermal Short Efficiency (9 runs)

References

1. Bendat, J.S., and A.G. Piersol, Random Data: Analysis and Measurement Procedures, Wiley-Interscience, New York, 1971.

2. Von Hoffmann, T. et al., "Experiments on Thermally Driven Gas Oscillation," Cryogenics, 1973.

Nomenclature

TAO

P	pressure at time t
P_o	initial pressure
T	temperature or period of data record
T_o	initial temperature
L/D	length/diameter ratio of tube
Re	acoustic Reynolds number

PSD

$x(t)$, $y(t)$	arbitrary functions of time
x_i, y_i	discrete values of $x(t)$, $y(t)$
$\overline{x}$, $\overline{y}$	mean values
ψ_x^2, ψ_y^2	mean square values
σ_x, σ_y	standard deviations
σ^2_x, σ^2_y	statistical variance
z_i	complex function $x_i + jy_i$
Z_k	Fourier transform of z
Z_k^*	complex conjugate of Z_k
G_x, G_y	power spectral density function
ϕ_x, ϕ_y	phase angle

Long Term Storage

A	area
$\overline{C}$	penetration conductance
$C_{p_{cryo}}$, $C_{p_{cry\ vapor}}$	specific heat of cryogen vapor at constant pressure
K_{MLI}	thermal conductivity of multilayer insulation perpendicular to the grain
K_{pene}	thermal conductivity of penetration channel
L	length of cylindrical section of the cryogenic storage tank
L_{pene}	length of penetration channel
$M_{Config.\,1}$	mass of Configuration 1, if total system mass of a cylindrical tank with spherical end caps surrounded by multilayer insulation, including cryogen, for specified conditions detailed in text
$M_{MLI_{2-3}}$	mass of multilayer insulation between layers defined by radii r_2 and r_3
$M_{pene_{2-3}}$	mass of penetrations through $M_{MLI_{2-3}}$
M_{total}	total system mass
M_{VCS}	mass of the vapor cooled shield
$\dot{m}_{cryo\ vapor}$, $\dot{m}_{cry}$	mass flow of cryogen vapor (boiloff)
q_{1-2}	heat transferred between radii r_1 and r_2
q_{2-3}	heat transferred between radii r_2 and r_3
q_{MLI}	heat transferred through multilayer insulation
$q_{MLI_{2-3}}$	heat transferred through multilayer insulation bounded by radii r_2 and r_3
$q_{pene_{2-3}}$	heat transferred through penetrations bounded by radii r_2 and r_3

q_1	heat transfer rate from ambient environment to shield or shroud
q_2	heat transfer rate to shield or shroud
q_3	heat transfer rate from shield or shroud to cryogen
$q_{VCS}, q_{V.S.}$	heat absorbed by the vapor cooled shield
r_1	inner radius of cryogen tank
r_2	radius for the vapor cooled shield
r_3	outer radius for Configuration 2 (cryogen tank with a vapor cooled shield)
T_{amb}	ambient temperature
T_1, T_2, T_3	temperature for r_1, r_2 and r_3 respectively
T_{cry}	temperature of stored cryogen
$thick_{wall}$	thickness of walls such as the tank wall and the vapor cooled shield wall
T_e	vapor temperature at exit of vapor cooled shield
T_{sh}	temperature of vapor cooled shield
$\eta_{shield}, \eta_{V.S.}$	vapor cooled shield heat transfer efficiency
$\eta_{t.s.}$	thermal short efficiency
ρ_{mat}	material density
T_p	temperature at thermal short

New Technology

The contract is being monitored continuously for new technology efforts that would be reportable under the contract clause entitled "New Technology." Any pertinent items will be reported under that clause.

Very truly yours,

LOCKHEED MISSILES & SPACE COMPANY, Inc.

Juan K. Lovin, Supervisor
Thermodynamics & Structures Section

JKL:WHS:jp

Attach: (1) References
(2) Nomenclature
(3) Financial Statement

Distribution:
AS21D, five copies
AT01 (Mr. Wiggins), one copy
EM34 (Mr. Bliss), one copy
EP43 (Mr. Hyde), eight copies
ES24 (Mr. Yates), one copy
ES24 (Dr. Urban), one copy
EH33 (Dr. Stuckey), one copy
EH32 (Mr. Austin), one copy
NASA-Lewis (Mr. Barber), one copy
NASA-KSC (Mr. Boggs), one copy
NASA-JSC (Mr. Chandler), one copy
NASA-S&TIF, one copy
GD/C (Mr. Tatro), one copy
NBS (Dr. Jones), one copy
NBS (Mr. Collier), one copy
Ball (Mr. Urbach), one copy
Ball (Dr. Davis), one copy
AES (Mr. Ahearn), one copy
LMSC-SV (Mr. Parmley), one copy
MMC (Mr. Hall), one copy
Air Res (Mr. Buchman), one copy
ACO (Mr. Van Brunt), one copy